An Efficient Hybrid Multi-Station TDOA and Single-Station AOA Localization Method

Xu Kang, Dejiang Wang, Yu Shao, Mingyang Ma, and Tao Zhang

***Abstract*— Multi-station passive localization algorithms based on hybrid Time Difference of Arrival (TDOA) and Angle of Arrival (AOA) have been thoroughly studied. But it usually requires each station to obtain the AOA of the source and relies on the precise station position. These conditions are generally not satisfied in practical applications. In addition, the geometry between the source and these stations also affects the localization accuracy. This paper studies the passive source localization problem based on multi-station TDOA and single-station AOA measurements. First, we propose a closed-form solution source localization method based on multi-station TDOA and single-station AOA measurements, which requires only the reference station used to calculate TDOA to be able to observe the AOA measurements of the source. It solves the problem of hybrid localization of different numbers of TDOA and AOA measurements. Theoretical analysis proves that the performance of the proposed method can reach the Cramer-Rao Lower Bound (CRLB) under small noise conditions. Then, we model the relationship between the position of each station relative to the source and the localization accuracy. Through the D-optimality criterion, we obtain the optimal geometry between multiple stations and the source Simulation results confirm the validity of these theories.**

***Index Terms*— Localization, time difference of arrival, angle of arrival, closed-form solution, Cramer-Rao lower bound, station position error, optimal geometry.**

I. Introduction

SOURCE localization is a fundamental problem in passive detection systems such as radar, sonar, wireless sensor networks, and communication systems. The localization process is performed by taking different types of measurements about the source from stations at known positions and then solving for the source position using a localization algorithm. In the past decades, various source localization methods have been proposed based on different types of measurements, such as time of arrival (TOA) [1], [2], time difference of arrival (TDOA) [3], [4], [5], angle of arrival (AOA) [6], [7], etc. and their combinations [8], [9], [10], [11], [12].

TDOA-based localization methods are often called hyperboloid localization, which estimates the source location through the intersection of several hyperboloids. AOA-based localization methods are often referred to as cross localization, which estimates the position of the source through the intersection of several rays. Localization methods based on their combinations estimate source locations through intersections between different hyperboloids and rays. The problem of source localization is often tough because the direct relationship between TDOA and AOA measurements and source location is non-linear and non-convex [13], [14]. Maximum Likelihood Estimation (MLE) is a general approach to this localization problem. MLE is asymptotically unbiased, and its performance can reach Cramer-Rao Lower Bound (CRLB) accuracy under Gaussian distributed noise conditions. However, MLE requires high-precision initial values for iterative computation, otherwise local convergence tends to occur. Therefore, we prefer to use source position estimation algorithms with closed-form solutions.

Closed-form solutions can effectively reduce computational complexity. References [3] and [15] studied TDOA localization algorithms with closed-form solutions. Reference [3] obtains a closed-form solution through nonlinear parameter transformation, whose performance can reach CRLB accuracy within a small error range under Gaussian noise conditions. Reference [15] compared two closed-form algorithms, spherical interpolation and spherical intersection and proved that the spherical intersection method is more suitable for passive localization. However, these methods may generate ghost points when the number of stations is small.

Much research has been done on passive localization using AOA [7], [16], [17]. In three-dimensional (3D) space, multiple pairs of azimuth and pitch angles are generally used for triangulation, which can determine the source position in the form of a closed solution. Under the condition of small noise obeying the zero-mean Gaussian independent and identically distributed (IID), its localization performance can reach CRLB. To further improve localization accuracy and robustness, many studies [10], [18], [19], [20], [21] proposed localization algorithms based on hybrid TDOA and AOA measurements. Reference [18] proposes a source localization method based on hybrid TDOA and AOA, which is more accurate than using TDOA and AOA alone. In [10], a constrained optimization method utilizing geometric constraints is applied

Manuscript received 12 July 2022; revised 14 November 2022; accepted 3 January 2023. Date of publication 17 January 2023; date of current version 14 August 2023. The associate editor coordinating the review of this article and approving it for publication was Y. Zhu. *(Corresponding author: Dejiang Wang.)*

Xu Kang, Yu Shao, and Tao Zhang are with the Changchun Institute of Optics Fine Mechanics and Physics Chinese Academy of Sciences, Changchun 130033, China, and also with the University of the Chinese Academy of Sciences, Beijing 101408, China (e-mail: xkang2019@163.com; shao61297@gmail.com; zhangt@ciomp.ac.cn).

Dejiang Wang and Mingyang Ma are with the Changchun Institute of Optics Fine Mechanics and Physics Chinese Academy of Sciences, Changchun 130033, China (e-mail: wangdj04@ciomp.ac.cn; ma7856728@163.com).

Color versions of one or more figures in this article are available at https://doi.org/10.1109/TWC.2023.3235753.

Digital Object Identifier 10.1109/TWC.2023.3235753

to hybrid TDOA-AOA localization, which is more robust than linear least squares.

Hybrid TDOA and AOA measurements can reduce the minimum number of stations required to localize the source. At least four stations are required to locate the source position in 3D space by TDOA. Based on the hybrid TDOA and AOA only two stations are required. In addition, it can reduce the number of stations required to achieve the desired positioning performance. Reference [19] proposed a closed-form localization method with hybrid TDOA and AOA measurements, which solved the problem of source localization under low probability of interception. Reference [21] introduced a structured total least squares method to further reduce the estimation bias of source locations.

In our research, the current localization algorithms based on hybrid TDOA and AOA require that each station can observe the AOA of the source. In fact, due to factors such as multipath effects, non-line-of-sight propagation, etc., observation stations sometimes cannot use infrared sensors or antenna arrays to obtain the AOA of the source. In addition, the high cost of antenna array receivers and infrared sensors diminishes the feasibility of mass use. These factors will cause the above algorithm to invalid.

To address the above problems, we delve into the localization model based on hybrid multi-station TDOA and single-station AOA measurements. We propose a closed-form solution localization algorithm by reconstructing the relationship between the measurements and the source position. When the station position error is also considered, we adopt a similar derivation to propose a robust closed-form solution positioning algorithm. Among them, we choose to use the station that can measure the source AOA as the reference station for calculating TDOA (unless otherwise stated below, the reference station represents the station that can obtain the source AOA). Under the condition of small noise obeying Gaussian distribution, the theoretical analysis proves that the performance of the above localization methods can reach CRLB accuracy.

In addition to localization algorithms, the geometry between the multi-stations and sources can also significantly affect the performance of source position estimation. References [22], [23], [24], [25], [26], and [27] study the optimal geometry between homogeneous sensors (sensors of the same type), such as TDOA, TOA, and AOA.

In practical applications, there are also different types of sensors working together to form a heterogeneous sensor network (HSN). By fusing information from different types of sensors, source localization can be achieved more easily and accurately. When hybrid TDOA and FDOA measurements are used to locate unknown radiation sources, [28] analyzed the effect of the geometry of the sensor relative to the source on the localization performance. Reference [29] investigated the optimal sensor placement problem for source localization by deploying two different types of sensors in HSN.

However, in studies based on hybrid TDOA and AOA measurement geometries, the background of study is generally that each station can only obtain TDOA or AOA from the source. In our investigation, the optimal geometry in the localization scenario of hybrid multi-station TDOA and single-station AOA measurements proposed in this paper has not been studied yet, and it has great practical significance. We model the relationship between the angular position of multi-station relative source and the localization performance. Through the D-optimality criterion, we give the optimal geometric configuration between the station and the source, which improves the positioning accuracy.

The rest of this article is organized as follows. Section II describes the localization scenario using multi-station TDOA and single-station AOA measurements. In Section III, we propose the corresponding closed-form solution source position estimator based on different noises and extend the usage scenarios. Section IV analyzes the performance and computational complexity of the proposed estimator. In Section V, we investigate the optimal geometric configuration of the source and these stations and give partial explicit solutions. Section VI verifies the theoretical results of the above sections through the numerical results. Section VII concludes this paper.

This paper uses bold uppercase letters and bold lowercase letters to denote matrices and column vectors, respectively. $[\mathbf{A}]_{i,j}$ is the i-th row and j-th column element of matrix $\mathbf{A}$. $\|\mathbf{a}\|$ is the Euclidean norm and $\rho_{\mathbf{a}} = \mathbf{a}/\|\mathbf{a}\|$ is the unit vector of $\mathbf{a}$. $\mathrm{diag}(\mathbf{a})$ is a diagonal matrix consisting of the elements of $\mathbf{a}$, $\mathrm{blkdiag}(\mathbf{A}, \ldots, \mathbf{B})$ is a block diagonal matrix consisting of $\mathbf{A}, \ldots, \mathbf{B}$. $\det(\mathbf{A})$ and $\mathrm{Tr}(\mathbf{A})$ represent the determinant and trace of $\mathbf{A}$, respectively. $\mathbf{I}$ and $\mathbf{O}$ are identity and zero matrices, and their subscripts indicate the matrix size. $\mathbf{1}_N$ and $\mathbf{0}_N$ are length N vectors of unity and zero. $(*)$ is the true value of the variable. $(\tilde{*})$ and $(\hat{*})$ represents the observed and estimated value of the variable $(*)$, respectively.

II. Localization Scenario

Fig. 1 depicts a scenario where multiple stations are used to locate sources in 3D space. The stations with known position $\mathbf{s}_i = [s_{x,i}, s_{y,i}, s_{z,i}]^T \in \mathbb{R}^3, i = 0, 1, 2, \ldots, N$ receive the reflected signal from the source with unknown position $\mathbf{u} = [u_x, u_y, u_z]^T \in \mathbb{R}^3$. A centralized pairing method is adopted between stations, and the measurements from all stations are transmitted to the reference station $\mathbf{s}_0$. That is, all stations are within the communication range of the reference station. Furthermore, all stations and the source are in a non-cooperative state.

The TDOA and AOA measurements received at each station are related to the location of the source as follows:

$$r_{i,0} = r_i - r_0, i = 1, 2, \ldots, N, \tag{1}$$

$$\alpha_0 = \arctan\left(\frac{u_y - s_{y,0}}{u_x - s_{x,0}}\right)$$

$$\beta_0 = \arctan\left(\frac{u_z - s_{z,0}}{l_0}\right) \tag{2}$$

where $r_{i,0}$ is the true range difference between the source and the two observation stations, $r_i = \|\mathbf{u} - \mathbf{s}_i\|$ and $r_0 = \|\mathbf{u} - \mathbf{s}_0\|$. Since the signal propagation speed is a constant, the TDOA and the range difference of arrival (RDOA) can be converted into each other and vice versa. In addition, since the value of TDOA is relatively small compared to AOA, when calculating the inverse or pseudo-inverse of the

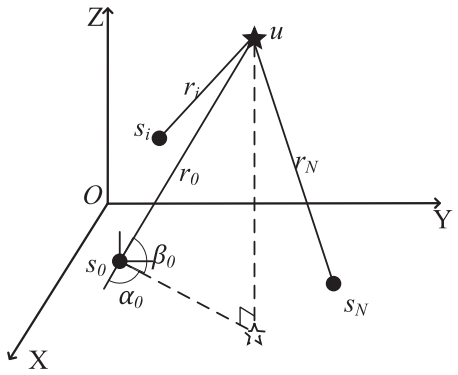

Fig. 1. Localization scenario.

matrix obtained from the measured values, the matrix may be close to singular values. Here we choose RDOA instead of TDOA to locate the source. $\arctan(*)$ is the arctangent function, and $l_0 = (u_x - s_{x,0})\cos\alpha_0 + (u_y - s_{y,0})\sin\alpha_0$ denotes the distance from the reference station to the source in the x-y plane where azimuth $\alpha_0 \in (-\pi, \pi]$ and elevation $\beta_0 \in [-\pi/2, \pi/2]$.

All measurements about the source are represented in vector form:

$$\tilde{\mathbf{m}} = \mathbf{m} + \mathbf{\Delta m}. \tag{3}$$

where $\tilde{\mathbf{m}}$ indicates $\mathbf{m}$ disturbed by noise, and $\mathbf{m} = \left[\mathbf{r}^T, \varphi_{\mathbf{0}}^T\right]^T \in \mathbb{R}^{N+2}$ represents the measurements corresponding to the real position of the source, where $\mathbf{r} = [r_{1,0}, r_{2,0}, \ldots, r_{N,0}]^T$ and $\varphi_{\mathbf{0}} = [\alpha_0, \beta_0]^T$. The measurement error vector $\mathbf{\Delta m} = [\Delta r_{1,0}, \ldots, \Delta r_{N,0}, \Delta\alpha_0, \Delta\beta_0] \in \mathbb{R}^{N+2}$ obeys the zero-mean Gaussian distribution and its covariance matrix [30], [31], which assumes that TDOA and AOA measurements are independent, is

$$\mathbf{Q_m} = \mathrm{blkdiag}\left(\mathbf{Q_r}, \mathbf{Q}_\varphi\right), \tag{4}$$

where $\mathbf{Q}_r = \sigma_{r_0}^2 \mathbf{1}_N \mathbf{1}_N^T + \mathrm{diag}\left(\left[\sigma_{r_1}^2, \sigma_{r_2}^2, \cdots, \sigma_{r_N}^2\right]\right) \in \mathbb{R}^{N\times N}$ and $\mathbf{Q}_\varphi = \mathrm{diag}\left(\left[\sigma_{\alpha_0}^2, \sigma_{\beta_0}^2\right]\right)$ are the covariance matrices of TDOA and AOA, respectively.

Our aim is to use the TDOA and AOA measurement vector $\tilde{\mathbf{m}}$ to estimate the unknown position $\mathbf{u}$ of the source as accurately and quickly as possible. In the next section, we propose localization methods with closed-form solutions based on different noises.

Remark 1: The moment when each station receives the reflected signal of the source does not coincide with the moment when the detection signal arrives at the source. Since the signal propagation speed is too fast, it is reasonable to take the estimated value of the source position at the moment of receiving the reflected signal at each station as the real position of the source at this time.

III. Localization Method

In this section, we derive a closed-form solution source position estimator for various noise scenarios. We combine (1) and (2) to linearize the TDOA and AOA measurements about the source position by clever deformation, and then estimate the source position using weighted least squares (WLS). We derive the localization technique in the presence of both measurement errors and station position errors and extend them to scenarios where multiple AOA measurements exist.

A. The Closed-form Solution for Source Position

We first investigate the localization method of closed-form solution in the presence of measurement errors. It is assumed that the exact station location is known.

Rewriting the distance difference formula as $r_{i,0} + \|\mathbf{u} - \mathbf{s}_0\| = \|\mathbf{u} - \mathbf{s}_i\|$, and squaring both sides to get

$$r_{i,0}^2 + \|\mathbf{s}_0\|^2 - \|\mathbf{s}_i\|^2 = 2(\mathbf{s}_0 - \mathbf{s}_i)^T\mathbf{u} + 2r_{i,0}r_0, \tag{5}$$

which is a linear function with respect to r_0 and $\mathbf{u}$. r_0 is the unknown variable associated with $\mathbf{u}$. Common methods for solving such functions are two-step weighted least squares (TSWLS) or semidefinite relaxation (SDR) with simultaneous estimation of unknown parameters and auxiliary variables [32]. These methods have relatively high computational complexity. In this paper, we reconstruct the relationship between TDOA measurements and the source position using the AOA obtained from the reference station, and use the WLS method to obtain the estimate of source in one step.

Using the AOA of the source observed at the reference station, we have [19]

$$\mathbf{u} - \mathbf{s}_0 = r_0\mathbf{b}, \tag{6}$$

where $\mathbf{b} = [\cos\beta_0\cos\alpha_0, \cos\beta_0\sin\alpha_0, \sin\beta_0]^T \in \mathbb{R}^3$ is the unit vector of the source relative to the reference station.

Multiplying both sides of (5) by at the same time to have

$$r_{i,0}^2 + \|\mathbf{s}_0\|^2 - \|\mathbf{s}_i\|^2 = 2(\mathbf{s}_0 - \mathbf{s}_i)^T\mathbf{u} - 2r_{i,0}\mathbf{b}^T r_0\mathbf{b}. \tag{7}$$

Substituting (6) into (7) to get

$$r_{i,0}^2 + \|\mathbf{s}_0\|^2 - \|\mathbf{s}_i\|^2 - 2r_{i,0}\mathbf{b}^T\mathbf{s}_0 = 2(\mathbf{s}_0 - \mathbf{s}_i - r_{i,0}\mathbf{b})^T\mathbf{u}, \tag{8}$$

which has only one unknown vector $\mathbf{u}$.

Stacking (8) for $i = 1, 2, \ldots, N$ and writing it as a matrix form

$$\mathbf{h_{mr}} = \mathbf{G_{mr}}\mathbf{u}, \tag{9}$$

where $\mathbf{h_{mr}} = \begin{bmatrix} r_{1,0}^2 + \|\mathbf{s}_0\|^2 - \|\mathbf{s}_1\|^2 - 2r_{1,0}\mathbf{b}^T\mathbf{s}_0 \\ \vdots \\ r_{N,0}^2 + \|\mathbf{s}_0\|^2 - \|\mathbf{s}_N\|^2 - 2r_{N,0}\mathbf{b}^T\mathbf{s}_0 \end{bmatrix} \in \mathbb{R}^N$, $\mathbf{G_{mr}} = 2\begin{bmatrix} (\mathbf{s}_0 - \mathbf{s}_1 - r_{1,0}\mathbf{b})^T \\ \vdots \\ (\mathbf{s}_0 - \mathbf{s}_N - r_{N,0}\mathbf{b})^T \end{bmatrix} \in \mathbb{R}^{N\times 3}$.

Now we deform (2), taking the tangent function on both sides of (2) at the same time, and denoting $\tan(*)$ as $\sin(*)/\cos(*)$, the cross product is obtained

$$\mathbf{h}_{\mathbf{m}\varphi} = \mathbf{G}_{\mathbf{m}\varphi}\mathbf{u}, \tag{10}$$

where $\mathbf{h}_{\mathbf{m}\varphi} = \gamma_{\mathbf{0}}^T\mathbf{s_0}$, $\mathbf{G}_{\mathbf{m}\varphi} = \gamma_{\mathbf{0}}^T$, and $\gamma_{\mathbf{0}} = \begin{bmatrix} \sin\alpha_0 & -\cos\alpha_0 & 0 \\ \sin\beta_0\cos\alpha_0 & \sin\beta_0\sin\alpha_0 & -\cos\beta_0 \end{bmatrix}^T \in \mathbb{R}^{3\times 2}$

Stacking (9) and (10) to get

$$\mathbf{h_m} = \mathbf{G_m u}, \tag{11}$$

where $\mathbf{h_m} = \left[\mathbf{h_{mr}^T}, \mathbf{h_{m\varphi}^T}\right]^T \in \mathbb{R}^{N+2}$, $\mathbf{G_m} = \left[\mathbf{G_{mr}^T}, \mathbf{G_{m\varphi}^T}\right]^T \in \mathbb{R}^{(N+2)\times 3}$.

(11) holds when $\mathbf{h_m}$ and $\mathbf{G_m}$ are expressed in terms of true measurements. However, in practice, the measurements are always disturbed by noise. In this case, $\tilde{\mathbf{h}}_\mathbf{m}$ and $\tilde{\mathbf{G}}_\mathbf{m}$ denote the regressors subject to noise interference. Through the first-order Taylor expansion, we get the pseudo-linear equality

$$\tilde{\mathbf{h}}_\mathbf{m} - \tilde{\mathbf{G}}_\mathbf{m}\mathbf{u} \simeq \varepsilon_\mathbf{m}, \tag{12}$$

where $\varepsilon_\mathbf{m} = \mathbf{T\Delta m} \in \mathbb{R}^{N+2}$ is the error term of the regression equation, $\mathbf{T} = \text{blkdiag}\left(\mathbf{T_r}, \mathbf{T}_\varphi\right)$, $\mathbf{T_r} = 2\text{diag}\left([r_1, r_2, \ldots, r_N]\right)$, and $\mathbf{T}_\varphi = \text{diag}\left([r_0 \cos\beta_0, r_0]\right)$.

From (12) we can get the WLS estimate of $\mathbf{u}$ as

$$\begin{aligned}\hat{\mathbf{u}}_\mathbf{m} &= \arg\min\left(\tilde{\mathbf{h}}_\mathbf{m} - \tilde{\mathbf{G}}_\mathbf{m}\mathbf{u}\right)^T \mathbf{W}\left(\tilde{\mathbf{h}}_\mathbf{m} - \tilde{\mathbf{G}}_\mathbf{m}\mathbf{u}\right) \\ &= (\tilde{\mathbf{G}}_\mathbf{m}^T\mathbf{W}\tilde{\mathbf{G}}_\mathbf{m})^{-1}\tilde{\mathbf{G}}_\mathbf{m}^T\mathbf{W}\tilde{\mathbf{h}}_\mathbf{m},\end{aligned} \tag{13}$$

where $\mathbf{W} = \left(\text{E}\left[\varepsilon_\mathbf{m}\varepsilon_\mathbf{m}^T\right]\right)^{-1} = \left(\mathbf{TQ_mT}^T\right)^{-1}$.

Remark 2: The weighting matrix $\mathbf{W}$ is unknown because it depends on the true position $\mathbf{u}$ of the source. In this regard, we can first replace $\mathbf{W}$ with the identity matrix or let $\mathbf{W} = \mathbf{Q_m}^{-1}$ to obtain the initial position estimate of the source [33], then use the initial position estimate to calculate a more accurate weighting matrix $\mathbf{W}$, and finally obtain the final solution by (13). Since the algorithm performance is insensitive to the approximation of the weight matrix, one or two iterations are sufficient to obtain an accurate position estimate of the source. If the condition number or rank of the estimated matrix is poor and we do not repeat, its solution degenerates to an ordinary least squares estimator (OLSE).

Remark 3: If matrix $\mathbf{G_m}$ is full rank and matrix $\mathbf{T}$ is invertible, the proposed method in this paper will get a unique solution. According to the definition of matrix $\mathbf{G_m}$ and $\mathbf{T}$, it is required that $\mathbf{s_0} - \mathbf{s_i} - r_{i,0}\mathbf{b} \neq 0$. That is, the source can appear in the middle of the line connecting stations, but not on the same side of the line connecting all the stations. The probability of this happening is almost 0, and it can be considered impossible.

B. Presence of Station Position Errors

In subsection A, our proposed source localization method requires precise station positions. Unfortunately, the station position is always disturbed by noise, and ignoring the station position error can result in a significant degradation in positioning performance [34]. We extend the closed-form solution for source locations to scenarios where station location errors exist.

The measurement error is uncorrelated with the station position error. We can derive the first-order noise term when only the measurement noise or the station position error exists, respectively, and then combine them to obtain a robust closed-form solution for the localization method when both errors exist.

We use $\tilde{\mathbf{s}}_i$ to denote the station position disturbed by noise

$$\tilde{\mathbf{s}}_i = \mathbf{s}_i + \Delta\mathbf{s}_i, i = 0, 1, 2, \ldots, N, \tag{14}$$

where $\Delta\mathbf{s} = \left[\Delta\mathbf{s}_0^T, \Delta\mathbf{s}_1^T, \ldots, \Delta\mathbf{s}_N^T\right]^T \in \mathbb{R}^{3N+3}$ is the station position error vector with zero mean Gaussian IID, its covariance matrix is

$$\mathbf{Q}_s = \text{blkdiag}\left(\mathbf{S}_0, \mathbf{S}_1, \cdots, \mathbf{S}_N\right) \in \mathbb{R}^{(3N+3)\times(3N+3)}, \tag{15}$$

where $\mathbf{S}_i = \text{diag}\left(\left[\sigma_{s_{i,x}}^2, \sigma_{s_{i,y}}^2, \sigma_{s_{i,z}}^2\right]\right)$.

Substituting (14) into (9) and (10) to get

$$\left[\tilde{\mathbf{h}}_\mathbf{sr}\right]_i - \left[\tilde{\mathbf{G}}_\mathbf{sr}\mathbf{u}\right]_i = -2r_i\rho_{\mathbf{u}-\mathbf{s_0}}^T\mathbf{\Delta s_0} + 2(\mathbf{u} - \mathbf{s_i})^T\mathbf{\Delta s_i}, \tag{16}$$

$$\tilde{\mathbf{h}}_{\mathbf{s}\varphi} - \tilde{\mathbf{G}}_{\mathbf{s}\varphi}\mathbf{u} = \gamma_\mathbf{0}^T\Delta\mathbf{s_0}. \tag{17}$$

Stacking (16) for $i = 1, 2, \ldots, N$ and (17) in matrix form

$$\tilde{\mathbf{h}}_\mathbf{s} - \tilde{\mathbf{G}}_\mathbf{s}\mathbf{u} = \mathbf{B\Delta s}, \tag{18}$$

where the subscript $\mathbf{s}$ indicates that it is only affected by the station position error, $\mathbf{B} = \left[\mathbf{B_r^T}, \mathbf{B}_\varphi^T\right]^T$, $\mathbf{B_r} = 2\left[\mathbf{B_{ra}}, \mathbf{B_{rb}}\right]$, $\mathbf{B_{ra}} = -[r_1, \cdots, r_N]^T \otimes \rho_{\mathbf{u}-\mathbf{s_0}}^T$, $\mathbf{B_{rb}} = \text{blkdiag}\left(\left[r_1\rho_{\mathbf{u}-\mathbf{s_1}}^T, r_2\rho_{\mathbf{u}-\mathbf{s_2}}^T, \ldots, r_N\rho_{\mathbf{u}-\mathbf{s_N}}^T\right]\right) \in \mathbb{R}^{N\times 3N}$, and $\mathbf{B}_\varphi = \left[\gamma_\mathbf{0}^T, \mathbf{O}_{2\times 3N}\right]$.

Considering both the measurement error and station position error, the equations (11) and (18) are combined, we get

$$\tilde{\mathbf{h}} - \tilde{\mathbf{G}}\mathbf{u} = \mathbf{T\Delta m} + \mathbf{B\Delta s}, \tag{19}$$

where $\tilde{\mathbf{h}}$ and $\tilde{\mathbf{G}}\mathbf{u}$ denote $\mathbf{h_m}$ and $\mathbf{G_m}$, respectively, which are affected by these two errors.

From (19) we can get the weighted least squares estimate of $\mathbf{u}$ as

$$\hat{\mathbf{u}}_\mathbf{b} = (\tilde{\mathbf{G}}^T\mathbf{\Sigma}\tilde{\mathbf{G}})^{-1}\tilde{\mathbf{G}}^T\mathbf{\Sigma}\tilde{\mathbf{h}}, \tag{20}$$

where $\Sigma = \left(E\left[(\mathbf{T\Delta m} + \mathbf{B\Delta s})(\mathbf{T\Delta m} + \mathbf{B\Delta s})^T\right]\right)^{-1} = \left(\mathbf{TQ_mT}^T + \mathbf{BQ_sB}^T\right)^{-1}$.

The *Remark* in this subsection refer to *Remark 2* and *Remark 3*.

C. MLE

MLE is a common method for solving nonlinear and nonconvex problems. It is asymptotically unbiased, but sensitive to initial values and has high computational complexity. When the noise powers are large, MLE will have the threshold effect [32]. Therefore, it is used as a comparison for the estimated performance of the proposed algorithm in this paper.

Below we briefly describe the estimation procedure of MLE. The maximum likelihood function is equivalent to the minimum cost function. From (3), the cost function is

$$J\left(\mathbf{u}\right) = \left(\tilde{\mathbf{m}} - \mathbf{m}\left(\mathbf{u}\right)\right)^T\mathbf{Q}_\mathbf{m}^{-1}\left(\tilde{\mathbf{m}} - \mathbf{m}\left(\mathbf{u}\right)\right), \tag{21}$$

where $\mathbf{m}\left(\mathbf{u}\right)$ is the measurement vector represented by the unknown variable $\mathbf{u}$. The minimization solution of the cost function (21) is usually obtained by the Gauss-Newton iterative method.

First, we take the true source position $\mathbf{u}$ as the initial iteration value $\mathbf{u}^0$, pseudo-linearize $\mathbf{m}\left(\mathbf{u}\right)$, and then find the

gradient of $J(\mathbf{u})$ and make it zero. The iterative process is as follows [35]:

$$\mathbf{u}^{k+1} = \mathbf{u}^k + \left(\nabla_{\mathbf{mu}}^T \mathbf{Q}_{\mathbf{m}}^{-1} \nabla_{\mathbf{mu}}\right)^{-1} \nabla_{\mathbf{mu}}^T \mathbf{Q}_{\mathbf{m}}^{-1} \left(\tilde{\mathbf{m}} - \mathbf{m}\left(\mathbf{u}^k\right)\right), \tag{22}$$

where $\mathbf{u}^k$ represents the value after k iterations, the number of iterations is related to the desired precision. $\nabla_{\mathbf{mu}}$ is the Jacobian of $\mathbf{m}(\mathbf{u})$ with respect to $\mathbf{u}$, where $\nabla_{\mathbf{mu}}$ is defined in (26).

We choose the true source position as the initial value of the iteration (which is impossible in practice) to prevent it from falling into a local optimum and to reduce the number of iterations. When station position error exists, the maximum likelihood estimates the source and station positions simultaneously. The process is similar to the above and will not be described here.

D. Presence of Multiple AOA

In order to enhance the localization performance, it is common to increase the number of AOA sensors in radar systems and wireless sensor networks. Based on the localization scenario in Section II, it is assumed that each station can observe the AOA vector, $\varphi_{\mathbf{i}} = [\alpha_i, \beta_i]^T \text{for} i = 1, 2, \cdots, N$, of the source. Similar to (2), the values of azimuth and pitch are:

$$\begin{aligned} \alpha_i &= \arctan\left(\frac{u_y - s_{y,i}}{u_x - s_{x,i}}\right) \\ \beta_i &= \arctan\left(\frac{u_z - s_{z,i}}{(u_x - s_{x,i})\cos\alpha_i + (u_y - s_{y,i})\sin\alpha_i}\right). \end{aligned} \tag{23}$$

From (8), only AOA measurement from the reference station is used in the linearization process of TDOA measurements concerning the source position. Therefore, we can deconstruct the measurements from other stations into AOA and TDOA and calculate them separately. In Section III-A, we have achieved the target localization using the AOA from the reference station and these TDOA measurements. For the remaining AOA measurement, we adopt the same processing method as the reference station. Obviously, it's easy to get the WLS estimate of $\mathbf{u}$ from all the measurements is

$$\hat{\mathbf{u}}_{\mathbf{n}} = (\tilde{\mathbf{G}}_{\mathbf{n}}^T \boldsymbol{\Sigma}_{\mathbf{n}} \tilde{\mathbf{G}}_{\mathbf{n}})^{-1} \tilde{\mathbf{G}}_{\mathbf{n}}^T \boldsymbol{\Sigma}_{\mathbf{n}} \tilde{\mathbf{h}}_{\mathbf{n}}. \tag{24}$$

The definitions of matrix $\tilde{\mathbf{G}}_{\mathbf{n}}$, $\boldsymbol{\Sigma}_{\mathbf{n}}$ and vector $\tilde{\mathbf{h}}_{\mathbf{n}}$ are given in Appendix A.

This localization technique can be applied to any number of stations carrying TDOA, AOA and their combination, when the reference station used to calculate the TDOA is able to observe the AOA measurement of the source. That is, the proposed method has strong robustness.

IV. Performance Analysis

In this section, we analyze the performance of the proposed method in terms of the mean square error (MSE) of the theoretical covariance matrix and the computational complexity of the algorithm.

The CRLB sets a bound on the variance of the unbiased estimate and is commonly used here to evaluate the performance of the unbiased estimators. In the previous section, we proposed closed-form source position estimators under different error conditions. To verify their performance, we compared the covariance matrix of the estimated solution with its corresponding CRLB. Then, we compare the computational complexity of the proposed closed-form solution localization method with MLE.

A. CRLB

First, we derive the CRLB under different noise conditions. For notational simplicity, we will use $\nabla_{\mathbf{ab}}$ to denote the partial derivative of the vector $\mathbf{a}$ with respect to the vector $\mathbf{b}$ at the true value, as

$$\nabla_{\mathbf{ab}} \underline{\underline{\text{def}}} \frac{\partial \mathbf{a}}{\partial \mathbf{b}^T}. \tag{25}$$

The measurement vector $\mathbf{m}$ is a function of the unknown parameter $\mathbf{u}$, and the measurement error obeys a zero-mean Gaussian distribution. When only the measurement error is considered, the CRLB of $\mathbf{u}$ is [36]

$$\text{CRLB}_{\mathbf{m}}(\mathbf{u}) = \left(\nabla_{\mathbf{mu}}^T \mathbf{Q}_{\mathbf{m}}{}^{-1} \nabla_{\mathbf{mu}}\right)^{-1}, \tag{26}$$

where $\nabla_{\mathbf{mu}} = \left[\nabla_{\mathbf{ru}}^T, \nabla_{\varphi\mathbf{u}}^T\right]^T$, $\nabla_{\mathbf{ru}} = [(\rho_{\mathbf{u}-\mathbf{s_1}} - \rho_{\mathbf{u}-\mathbf{s_0}}), \ldots, (\rho_{\mathbf{u}-\mathbf{s_N}} - \rho_{\mathbf{u}-\mathbf{s_0}})]^T \in \mathbb{R}^{N\times 3}$, $\nabla_{\varphi\mathbf{u}} = \frac{1}{r_0}\begin{bmatrix} \sin\alpha_0/\cos\beta_0 & -\cos\alpha_0/\cos\beta_0 & 0 \\ \sin\beta_0\cos\alpha_0 & \sin\beta_0\sin\alpha_0 & -\cos\beta_0 \end{bmatrix} \in \mathbb{R}^{2\times 3}$.

Similarly, when considering both measurement noises and station position errors, the CRLB of the parameter vector $\theta = \left[\mathbf{u}^T, \mathbf{s}^T\right]^T$ is [36]

$$\text{CRLB}_{\mathbf{b}}(\theta) = \begin{bmatrix} \nabla_{\mathbf{mu}}^T \mathbf{Q}_{\mathbf{m}}^{-1} \nabla_{\mathbf{mu}} & \nabla_{\mathbf{mu}}^T \mathbf{Q}_{\mathbf{m}}^{-1} \nabla_{\mathbf{ms}} \\ \nabla_{\mathbf{ms}}^T \mathbf{Q}_{\mathbf{m}}^{-1} \nabla_{\mathbf{mu}} & \nabla_{\mathbf{ms}}^T \mathbf{Q}_{\mathbf{m}}^{-1} \nabla_{\mathbf{ms}} + \mathbf{Q}_{\mathbf{s}}^{-1} \end{bmatrix}^{-1}, \tag{27}$$

where $\nabla_{\mathbf{ms}} = \left[\nabla_{\mathbf{rs}}^T, \nabla_{\varphi\mathbf{s}}^T\right]^T$, $\nabla_{\mathbf{rs}} = \left[\rho_{\mathbf{u}-\mathbf{s_0}}^T \otimes \mathbf{1}_N, \mathbf{R}_{\mathbf{s}}\right] \in \mathbb{R}^{N\times 3(N+1)}$, $\mathbf{R}_{\mathbf{s}} = -\text{blkdiag}\left(\rho_{\mathbf{u}-\mathbf{s_1}}^T, \rho_{\mathbf{u}-\mathbf{s_2}}^T, \cdots, \rho_{\mathbf{u}-\mathbf{s_N}}^T\right)$, $\nabla_{\varphi\mathbf{s}} = [\nabla_{\varphi\mathbf{u}}, \mathbf{O}_{2\times 3N}] \in \mathbb{R}^{2\times 3(N+1)}$.

The CRLB of $\mathbf{u}$ is the upper left 3×3 part of the matrix of the above formula. Using the block matrix inversion formula to obtain

$$\begin{aligned} \text{CRLB}_{\mathbf{b}}(\mathbf{u})^{-1} = {} & \nabla_{\mathbf{mu}}^T \mathbf{Q}_{\mathbf{m}}^{-1} \nabla_{\mathbf{mu}} - \nabla_{\mathbf{mu}}^T \mathbf{Q}_{\mathbf{m}}^{-1} \nabla_{\mathbf{ms}} \\ & \times \left(\nabla_{\mathbf{ms}}^T \mathbf{Q}_{\mathbf{m}}^{-1} \nabla_{\mathbf{ms}} + \mathbf{Q}_{\mathbf{s}}^{-1}\right)^{-1} \nabla_{\mathbf{ms}}^T \mathbf{Q}_{\mathbf{m}}^{-1} \nabla_{\mathbf{mu}}. \end{aligned} \tag{28}$$

B. Performance of The Proposed Method

In the process of calculating the weighting matrix, we ignore the second-order and above high-order measurement noise terms. The pseudo-linear equality for (12) and (19) is feasible when the following small error conditions are satisfied C1) $\Delta r_{i,0}/r_{i,0} \simeq 0$ for $i = 0, 1, \ldots, N$, C2) $\Delta\alpha_0 = \tilde{\alpha}_0 - \alpha_0 \approx 0$, C3) $\Delta\beta_0 = \tilde{\beta}_0 - \beta_0 \approx 0$, C4) $\left\|\text{diag}(\mathbf{s_i})^{-1} \Delta\mathbf{s_i}\right\| \simeq 0$ for $i = 0, 1, \ldots, N$.

Since $\mathbf{u}$ can be written in the form of $(\tilde{\mathbf{G}}_\mathbf{m}^T\mathbf{W}\tilde{\mathbf{G}}_\mathbf{m})^{-1}\tilde{\mathbf{G}}_\mathbf{m}^T\mathbf{W}\tilde{\mathbf{G}}_\mathbf{m}\mathbf{u}$, through (12) and (13), we can get the estimated bias of $\mathbf{u}$ as

$$\Delta\mathbf{u_m} = \hat{\mathbf{u}}_\mathbf{m} - \mathbf{u} = (\tilde{\mathbf{G}}_\mathbf{m}^T\mathbf{W}\tilde{\mathbf{G}}_\mathbf{m})^{-1}\tilde{\mathbf{G}}_\mathbf{m}^T\mathbf{W}\varepsilon_\mathbf{m}, \tag{29}$$

$\Delta\mathbf{u_m}$ follows a zero-mean Gaussian distribution, and its covariance matrix is

$$\begin{aligned}\mathrm{cov}_\mathbf{m}(\mathbf{u}) &= \mathrm{E}\left[\boldsymbol{\Delta}\mathbf{u_m}\boldsymbol{\Delta}\mathbf{u}_\mathbf{m}^T\right] = (\tilde{\mathbf{G}}_\mathbf{m}^T\mathbf{W}\tilde{\mathbf{G}}_\mathbf{m})^{-1} \\ &\simeq (\mathbf{G_m}^T\mathbf{W}\mathbf{G_m})^{-1}.\end{aligned} \tag{30}$$

Substituting $\mathbf{W} = \left(\mathbf{T}\mathbf{Q_m}\mathbf{T}^T\right)^{-1}$, (30) becomes

$$\mathrm{cov}_\mathbf{m}(\mathbf{u}) = \left[(\mathbf{T}^{-1}\mathbf{G_m})^T\mathbf{Q}_\mathbf{m}^{-1}\mathbf{T}^{-1}\mathbf{G_m}\right]^{-1}. \tag{31}$$

Similar to (29), estimation bias of the source position $\mathbf{u}$ is:

$$\Delta\mathbf{u_b} = \hat{\mathbf{u}}_\mathbf{b} - \mathbf{u} = (\tilde{\mathbf{G}}^T\boldsymbol{\Sigma}\tilde{\mathbf{G}})^{-1}\tilde{\mathbf{G}}^T\boldsymbol{\Sigma}\left(\mathbf{T}\boldsymbol{\Delta}\mathbf{m} + \mathbf{B}\boldsymbol{\Delta}\mathbf{s}\right), \tag{32}$$

the covariance matrix for the bias is

$$\begin{aligned}\mathrm{cov}_\mathbf{b}(\mathbf{u}) &= \mathrm{E}\left[\boldsymbol{\Delta}\mathbf{u_b}\boldsymbol{\Delta}\mathbf{u}_\mathbf{b}^T\right] = (\tilde{\mathbf{G}}^T\boldsymbol{\Sigma}\tilde{\mathbf{G}})^{-1} \simeq (\mathbf{G}^T\Sigma\mathbf{G})^{-1} \\ &= \left(\mathbf{G}^T\left(\mathbf{T}\mathbf{Q_m}\mathbf{T}^T + \mathbf{B}\mathbf{Q_s}\mathbf{B}^T\right)^{-1}\mathbf{G}\right)^{-1}.\end{aligned} \tag{33}$$

Through some algebraic operations, Appendix B proves that (31) and (33) are equivalent to (26) and (28), respectively. In other words, under conditions (C1)–(C4) and over the small error region, the performance of our proposed closed-form solution localization method can reach CRLB.

C. Computational Complexity

Next, we evaluated the computational complexity of the proposed WLS algorithm and compared it with OLSE and MLE, where WLS and MLE require initial solutions. *Remark 2* mentions that WLS is not sensitive to the initial value and can be replaced by an OLSE solution. MLE is very dependent on the initial value. We choose the real source position as the initial value to ensure positioning performance and reduce the number of iterations.

The computational complexity of MLE depends on the number of iterations. For a nonlinear problem with m equations and n unknown variables, the computational complexity of each iteration $(m \gg n)$ of the Gauss-Newton method is $O\left(km^3\right)$, where k is the number of iterations [36]. In the positioning scenario in Section III-A, the computational complexity of MLE is approximately equal to

$$O\left(k(N+2)^3\right). \tag{34}$$

In the same positioning scenario, the computational complexity of the weighted least squares algorithm is $O\left(2m^2n + mn^2 + mn + n^3 + n^2\right)$ [37]. For (13) and (20), their computational complexity is

$$O\left(6\left(N^2 + 4N + 14\right)\right). \tag{35}$$

When $m > 2n$, the upper bound on the computational complexity of the WLS algorithm is $O\left(m^3\right)$. Obviously, the computational complexity of the proposed WLS estimator is lower than that of MLE.

When the station position error exists, MLE needs to estimate not only the source position but also the station position. It generates high computational complexity. At the same time, iteration makes its computational complexity much higher than WLS, hence we will not analyze it in detail here.

V. Optimal Geometry

The positioning accuracy depends not only on the measurement noise, but also on the geometry between the source and the stations. Better positioning accuracy can be obtained by optimizing the placement configuration. To complete the study and further improve the localization accuracy, in this section, we derive the optimal geometry between the station and the source that maximizes source localization accuracy.

Typically, the A-optimality, D-optimality, and E-optimality criteria are used to determine the optimal geometric layout. These criteria are functions of different forms represented by eigenvalues of the CRLB matrix, and they are well compared in [38]. An important advantage of D-optimality is that it is invariant under scale changes in the parameters and linear transformations of the output, whereas A-optimality and E-optimality are affected by these transformations [39]. Here, we choose to use the D-optimality criterion: the product of eigenvalues is minimized. It is equivalent to maximize the determinant of information matrix., Our aim is to find the geometry configurations that satisfy the D-optimality criterion.

For ease of analysis, we consider the scenario where $N+1$ stations locate the source in the 2-D plane, where only $\mathbf{s_0}$ is the reference station. Without loss of generality, we set the source to be the origin of the coordinates as shown in Fig. 2. Setting the angular position of the i-th station relative to the source as λ_i, $\lambda_i \in [0°, 360°), \forall i = 0, 1, 2, \cdots, N$. The optimal geometry is denoted by λ_i.

(26) gives the Fisher information matrix (FIM) of the source position estimation in the 2D plane as

$$\mathrm{FIM} = \nabla'_{\mathbf{ru}}{}^T\mathbf{Q_r}^{-1}\nabla'_{\mathbf{ru}} + \nabla'_{\varphi\mathbf{u}}{}^T\mathbf{Q}_{\varphi\mathbf{0}}{}^{-1}\nabla'_{\varphi\mathbf{u}}. \tag{36}$$

The Jacobian matrix and its components in (26), represented by the angular position λ_i, are simplified as $\nabla'_{\mathbf{ru}} = \left[(\rho'_{\mathbf{u-s_1}} - \rho'_{\mathbf{u-s_0}}), \ldots, (\rho'_{\mathbf{u-s_N}} - \rho'_{\mathbf{u-s_0}})\right]^T$, $\rho'_{\mathbf{u-s}_i} = [\cos\lambda_i, \sin\lambda_i]^T$ and $\nabla'_{\varphi\mathbf{u}} = \frac{1}{r_0}[\sin\lambda_0, -\cos\lambda_0]$. Therefore, substituting (36) and simplifying to get

$$\mathbf{A} = \begin{bmatrix} A_{11} & A_{12} \\ A_{21} & A_{22} \end{bmatrix}, \tag{37}$$

where $A_{11} = \sum_{i=0}^{N}\frac{\cos^2\lambda_i}{\sigma_{r_i}^2} - \frac{1}{N_{\sigma_r}}\left(\sum_{i=0}^{N}\frac{\cos\lambda_i}{\sigma_{r_i}^2}\right)^2 + \frac{\sin^2\lambda_0}{r_0^2\sigma_{\alpha_0}^2}$, $A_{22} = \sum_{i=0}^{N}\frac{\sin^2\lambda_i}{\sigma_{r_i}^2} - \frac{1}{N_{\sigma_r}}\left(\sum_{i=0}^{N}\frac{\sin\lambda_i}{\sigma_{r_i}^2}\right)^2 + \frac{\cos^2\lambda_0}{r_0^2\sigma_{\alpha_0}^2}$, $A_{12} = A_{21} = \sum_{i=0}^{N}\frac{\cos\lambda_i\sin\lambda_i}{\sigma_{r_i}^2} - \frac{1}{N_{\sigma_r}}\sum_{i=0}^{N}\frac{\cos\lambda_i}{\sigma_{r_i}^2}\sum_{i=0}^{N}\frac{\sin\lambda_i}{\sigma_{r_i}^2} - \frac{\cos\lambda_0\sin\lambda_0}{r_0^2\sigma_{\alpha_0}^2}$, and $N_{\sigma_r} = \sum_{i=0}^{N}\frac{1}{\sigma_{r_i}^2}$.

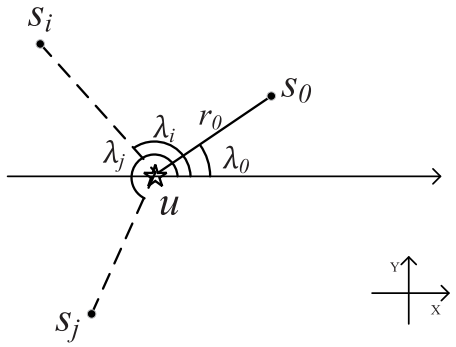

Fig. 2. Angular position of each station relative to the source.

If the geometric configuration of the source and stations rotates counterclockwise around the source in the 2D plane, the new FIM is

$$\mathbf{A}' = \mathbf{R}(\delta)^T \mathbf{A} \mathbf{R}(\delta), \tag{38}$$

where $\mathbf{R}(\delta) = \begin{bmatrix} \cos\delta & -\sin\delta \\ \sin\delta & \cos\delta \end{bmatrix}$ is the rotation matrix.

According to Cauchy-Binet formula, we get

$$\det(\mathbf{A}') = \det(\mathbf{A}). \tag{39}$$

In other words, we conclude that the determinant of FIM is invariant for rotation in the 2D plane. For the convenience of calculation, we set the angular position of the reference station to be $\lambda_0 = 0°$. The determinant of FIM expands to get

$$\begin{aligned}
&\det(\mathbf{A}) \\
&= A_{11}A_{22} - A_{12}^2 \\
&= \left[\sum_{i=0}^{N} \frac{\cos^2\lambda_i}{\sigma_{r_i}^2} - \frac{1}{N_{\sigma_r}}\left(\sum_{i=0}^{N} \frac{\cos\lambda_i}{\sigma_{r_i}^2}\right)^2\right] \\
&\quad \times \left[\sum_{i=0}^{N} \frac{\sin^2\lambda_i}{\sigma_{r_i}^2} - \frac{1}{N_{\sigma_r}}\left(\sum_{i=0}^{N} \frac{\sin\lambda_i}{\sigma_{r_i}^2}\right)^2 + \frac{1}{r_0^2\sigma_{\alpha_0}^2}\right] \\
&\quad - \left(\sum_{i=0}^{N} \frac{\cos\lambda_i \sin\lambda_i}{\sigma_{r_i}^2} - \frac{1}{N_{\sigma_r}} \sum_{i=0}^{N} \frac{\cos\lambda_i}{\sigma_{r_i}^2} \sum_{i=0}^{N} \frac{\sin\lambda_i}{\sigma_{r_i}^2}\right)^2 \\
&\leq \left[\sum_{i=0}^{N} \frac{\cos^2\lambda_i}{\sigma_{r_i}^2} - \frac{1}{N_{\sigma_r}}\left(\sum_{i=0}^{N} \frac{\cos\lambda_i}{\sigma_{r_i}^2}\right)^2\right] \\
&\quad \times \left[\sum_{i=0}^{N} \frac{\sin^2\lambda_i}{\sigma_{r_i}^2} + \frac{1}{r_0^2\sigma_{\alpha_0}^2}\right].
\end{aligned} \tag{40}$$

The equation holds when the angular position of each station satisfies the following conditions

$$\begin{aligned}
\sum_{i=0}^{N} \frac{\cos\lambda_i \sin\lambda_i}{\sigma_{r_i}^2} &= 0 \\
\sum_{i=0}^{N} \frac{\sin\lambda_i}{\sigma_{r_i}^2} &= 0.
\end{aligned} \tag{41}$$

To obtain an explicit solution, we consider the special case of equal measurement noise variances, i.e.: $\sigma_{r_0}^2 = \sigma_{r_1}^2 = \cdots = \sigma_{r_N}^2 = \sigma_r^2$, $\sigma_{\alpha_0} = \sigma_\varphi$.

(40) can be simplified as

$$\begin{aligned}
&\det(\mathbf{A}) \\
&\leq \frac{1}{\sigma_r^4}\left[\sum_{i=0}^{N} \cos^2\lambda_i - \left(\sum_{i=0}^{N} \cos\lambda_i\right)^2 \Big/ (N+1)\right] \\
&\quad \times \left[\sum_{i=0}^{N} \sin^2\lambda_i\right] \\
&\quad + \frac{1}{r_0^2\sigma_\varphi^2\sigma_r^2}\left[\sum_{i=0}^{N} \cos^2\lambda_i - \left(\sum_{i=0}^{N} \cos\lambda_i\right)^2 \Big/ (N+1)\right].
\end{aligned} \tag{42}$$

(42) consists of two parts, but the optimal geometric configurations of the two parts are different. The optimal geometric configuration of the first half and the second half are uniform angle array (UAA), $\lambda_i = 2\pi i/(N+1) + \lambda_0, i = 0, 1, \cdots, N$, and $\lambda_i = \left[1 - (-1)^i\right]\pi/2 + \lambda_0, i = 0, 1, \cdots, N$, respectively. It is difficult to obtain the general solution of the optimal layout because it is also affected by parameters σ_r, σ_φ, and r_0. In Appendix C we derive the following conclusions about the optimal geometric configuration.

Conclusion 1: When two stations $(N = 1)$ cooperatively locate, the optimal geometry is such that station $\mathbf{s_1}$ is located on the extension line of the reference station pointing to the source, i.e. $\lambda_1 = \pi + \lambda_0$. The distance between the source and the reference station should also be as small as possible when objective conditions allow, the same below.

Conclusion 2: When three stations $(N = 2)$ cooperatively locate and $r_0 \leq \frac{\sigma_r}{2\sigma_\varphi}$, the optimal geometric configuration is that three stations are collinear and the source is located between stations, i.e. $(\lambda_1, \lambda_2) \in \{(\pi + \lambda_0, \pi + \lambda_0), (\lambda_0, \pi + \lambda_0)\}$. If $r_0 > \frac{\sigma_r}{2\sigma_\varphi}$, the optimal geometric layout is $\lambda_1 = \cos^{-1}a + \lambda_0$ and $\lambda_2 = 2\pi - \cos^{-1}a + \lambda_0$, where $a = 1/4 - \sqrt{9/16 + \sigma_r^2/\left(4r_0^2\sigma_\varphi^2\right)}$.

If the number of stations participating in localization is greater than four, it is quite complicated to analyze the optimal sensor configuration under the localization model of this paper, and there is no intuitive solution for this situation. When the values of parameters σ_r, σ_φ and r_0 are determined, we can express the optimal geometric configuration problem (40) as an optimization problem with constraints. One method is the gradient search method which uses unknown variables for initial value guessing but may fall into the local optimum. Another method uses a search algorithm, such as particle swarm optimization, but its computational complexity increases rapidly with the increase in the number of stations, which is not suitable for multi-station localization.

Remark 4: The relationship between the error ellipse probable and the determinant of the FIM is $S_{EEP} = \pi \Big/ \sqrt{\det(\mathrm{FIM})}$ [38]. According to (40), the determinant of FIM is negatively correlated with the measurement noise variance but positively correlated with the number of stations.

TABLE I
POSITIONS OF THE STATIONS IN SIMULATIONS (M)

x	300	-300	300	-300	300	-300	300	-300
y	400	-400	-400	400	400	-400	-400	400
z	500	-500	500	-500	-500	500	-500	500

We can improve the source location accuracy by increasing the number of stations or using higher precision sensors.

VI. SIMULATION

In this section, we evaluate the performance of the proposed method and the conclusion of the optimal geometric configuration through Monte Carlo numerical simulation experiments. The simulation results are displayed in the form of root mean square error (RMSE) and estimated bias, where $\mathrm{RMSE}(\mathbf{u}) = \sqrt{\sum_{i=1}^{L} \|\hat{\mathbf{u}}_i - \mathbf{u}\|^2 / L}$ and $\mathrm{bias}(\mathbf{u}) = \sqrt{\left\| \sum_{i=1}^{L} \hat{\mathbf{u}}_i / L - \mathbf{u} \right\|^2}$, where $\mathbf{u}$ is the true source position and $\hat{\mathbf{u}}_i$ is the estimated value obtained from the i-th simulation. $L = 5000$ is the number of Monte Carlo experiments.

A. Localization Performance Varies With Noise

The performance of the localization technique proposed in this paper is analyzed in terms of both measurement noise and station position error. The TDOA measurement noise, AOA measurement noise and station position error are independent. The variances of measurement noise and station position errors in covariance matrices $\mathbf{Q_r}$, $\mathbf{Q}_\varphi$ and $\mathbf{Q_s}$ satisfy $\sum_{i=0}^{N} \sigma_{r_i}^2 \Big/ (N+1) = \sigma_r^2$, $\sum_{i=0}^{N} \left(\sigma_{\alpha_i}^2 + \sigma_{\beta_i}^2\right) \Big/ (N+1) = 2\sigma_\varphi^2$ and $\sum_{i=0}^{N} \left(\sigma_{s_{i,x}}^2 + \sigma_{s_{i,y}}^2 + \sigma_{s_{i,z}}^2\right) \Big/ (N+1) = 3\sigma_s^2$, respectively, where σ_r, σ_φ and σ_s are scaling constants [17].

Representing the axes on a logarithmic scale covers a larger dynamic range for better visualization. The range of the AOA measurement noise level σ_φ is from -10 to 20, corresponding to $1/e\,\mathrm{deg}$ and $e^2\,\mathrm{deg}$ and that of σ_r is from -10 to 50, corresponding to $1/e\mathrm{m}$ and $e^5\mathrm{m}$. The range of the station position error level σ_s is also from -10 to 50, corresponding to $1/e\mathrm{m}$ and $e^5\mathrm{m}$.

First, we verify the localization performance and computational complexity of the proposed algorithm through simulation experiments. The CRLB root, OLSE and IMLE are used as benchmark for performance evaluation, where IMLE denotes the MLE initialized with the true source position.

Scenario 1: We use these stations in Table I to locate source $\mathbf{u^o} = [1000, 1000, 1000]^T\mathrm{m}$, where the first station is the reference station. The remaining stations can only be used to calculate TDOA.

Fig. 3 shows the performance of the proposed method as σ_r varies. When σ_r is small, both our proposed method and IMLE outperform OLSE and can achieve CRLB accuracy. The bias of the solution of our proposed method is quite minor relative to RMSE, which is approximately an unbiased estimate. Compared with (a), the error in the first half of (b) comes from the position error $\sigma_s = 5\mathrm{m}$. The RMSE of the proposed method increases gradually with the increase of

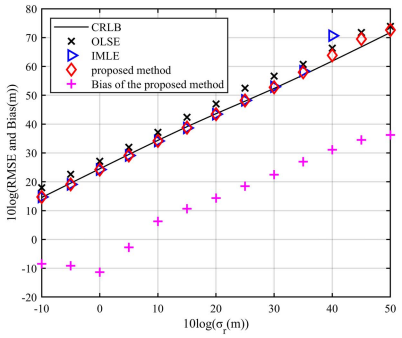

(a)

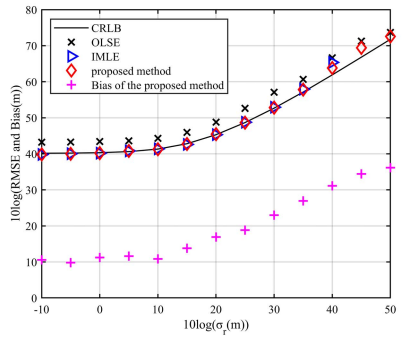

(b)

Fig. 3. Performance of the source localization as σ_r increases, where $\sigma_\varphi = 1^\circ$; (a) $\sigma_s = 0\mathrm{m}$; (b) $\sigma_s = 5\mathrm{m}$.

TABLE II
THE AVERAGE RUNNING TIME OF THE CONSIDERED ALGORITHMS

Algorithm	proposed	OLSE	IMLE
Time(ms)	0.42	0.16	7.4

noise. When $\sigma_r \approx 90\mathrm{m}$, there is a threshold effect in IMLE. It is probably due to the fact that the observation error surface near the true source location is irregular and susceptible to noise interference. However, our proposed algorithm still has good performance at this time.

Fig. 4 illustrates the performance of the proposed method as σ_φ varies. Similar to Fig. 3, when the noise is small, the proposed method outperforms OLSE and can achieve CRLB accuracy, and is approximately an unbiased estimate. But we find that changes in σ_φ have little effect on the proposed method and the corresponding CRLB. This is because the number of TDOA measurements is much larger than AOA measurements, which has a greater impact on the estimation results.

When the station position error does not exist, we roughly estimate the computational complexity of these algorithms through Intel Core-i7 CPU runtime, as shown in Table II. As mentioned in *Remark 2*, the proposed method requires one or two iterations to obtain the exact weighting matrix, resulting in its computational complexity being slightly higher than OLSE, but still much lower than IMLE. Notably, the average number of IMLE iterations is 11.2.

Scenario 2: The parameter settings for source and station are the same as in *Scenario 1*. We set the standard deviation

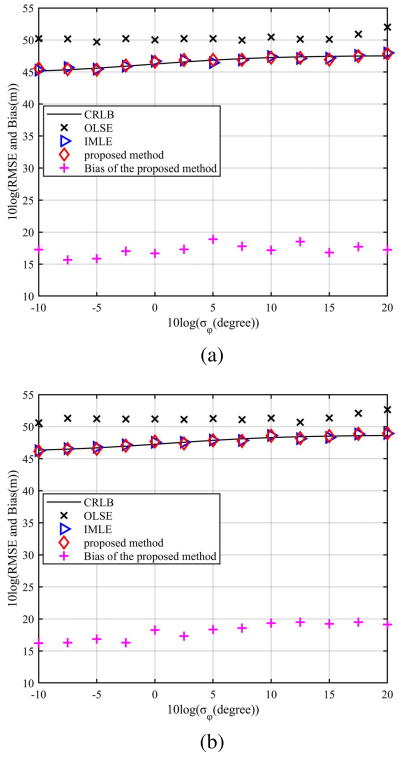

Fig. 4. Performance of the source localization as σ_φ increases, where $\sigma_\mathrm{r} = 10\mathrm{m}$; (a) $\sigma_s = 0\mathrm{m}$; (b) $\sigma_s = 5\mathrm{m}$.

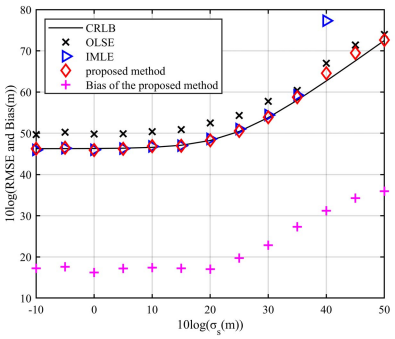

Fig. 5. Performance of the source localization as σ_s increases, where $\sigma_\mathrm{r} = 10\mathrm{m}$ and $\sigma_\varphi = 1^\circ$.

of the measurement noise as $\sigma_r = 10\mathrm{m}$ and $\sigma_\varphi = 1^\circ$, and then analyzed the influence of station position error on the localization performance.

Fig. 5 shows the performance of the proposed method as σ_s varies. The trend of performance evolution is consistent with Fig. 3-(b). In particular, when $\sigma_s \approx 55\mathrm{m}$, the IMLE appears threshold effect. Since σ_r only affects the weighting matrix of TDOA, while σ_s determines the weighting matrix of both TDOA and AOA.

Scenario 3: Setting the station positions and noise distribution are the same as *Scenario 1*. However, some of the stations carry different types of sensors, where stations $\mathbf{s}_6$ and $\mathbf{s}_7$ are loaded with only AOA sensors and are not used to calculate TDOA.

Under different noise conditions, the proposed localization method is compared with the algorithms based on various measurements, i.e. (i) MPR-TDOA: the TDOA

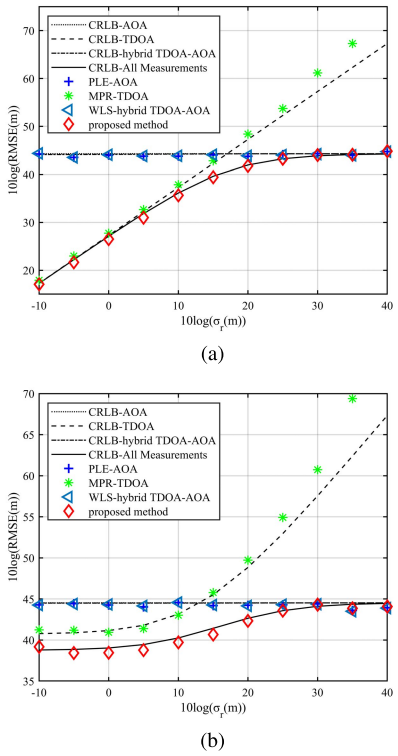

Fig. 6. Localization performance of different algorithms as σ_r increases, where $\sigma_\varphi = 1^\circ$; (a) $\sigma_s = 0\mathrm{m}$; (b) $\sigma_s = 5\mathrm{m}$.

closed-form solution based on the modified polar representation [40]; (ii) PLE-AOA: the AOA pseudolinear estimator [17]; and (iii) WLS-hybrid (TDOA-AOA): the weighted least squares algorithm based on hybrid TDOA and AOA measurements [19].

The three algorithms use various measurements, CRLB-AOA, CRLB-TDOA and CRLB-hybrid TDOA-AOA represent the lower bounds of localization performance based on AOA, TDOA and their mixture, respectively. Section III-D describes the robustness of our algorithm. Similarly, the WLS-hybrid can also be used in hybrid measurement scenarios where AOA measurements are added [19]. MPR-TDOA and PLE-AOA are not compatible with measurements from heterogeneous sensors.

Furthermore, the estimation biases of these algorithms are negligible relative to their RMSEs and will not be discussed here. We use the method in Section III-B to expand the impact of station position errors on the localization performance of these algorithms.

The proposed method proposed can take advantage of all the measurements in *Scenario 3* and therefore has a lower CRLB. With the increase of TDOA noise, MPR-TDOA gradually deviates from the corresponding CRLB, and PLE-AOA is not affected as show in Fig.6. The WLS-hybrid can utilize few TDOA compared to AOA, so the localization performance is similar to PLE-AOA. When the TDOA noise is very high, the AOA measurement guarantees the positioning performance of WLS-hybrid and our closed-form estimator. When the station position error is $\sigma_s = 5\mathrm{m}$, the RMSE of our algorithm is smaller under small TDOA noise.

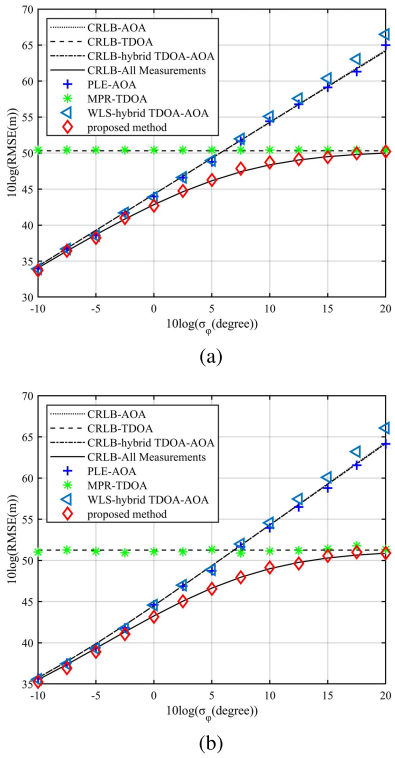

Fig. 7. Localization performance of different algorithms as σ_φ increases, where $\sigma_r = 10\text{m}$; (a) $\sigma_s = 0\text{m}$; (b) $\sigma_s = 5\text{m}$.

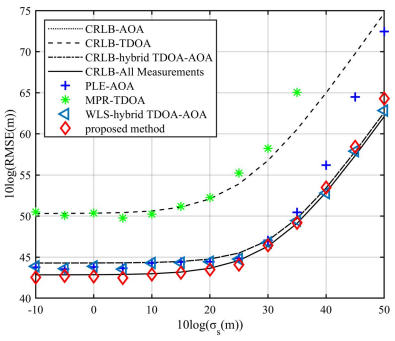

Fig. 8. Localization performance of different algorithms as σ_s increases, where $\sigma_\text{r} = 10\text{m}$ and $\sigma_\varphi = 1^\circ$.

As the AOA noise increases, the simulation results in Fig. 7 are similar to those in Fig. 6. The RMSE of PLE-AOA and WLS-hybrid increases gradually while MPR-TDOA remains unchanged. The proposed method can make full use of TDOA measurements to reduce the influence of AOA noise.

Then, we investigate the effect of station position error on these algorithms, as Fig. 8. With the increase of σ_s, MPR-TDOA and PLE-AOA deviate from the corresponding CRLB. WLS-hybrid and our algorithm always achieve CRLB accuracy very well. In other words, the hybrid measurement model is more resistant to station position error.

The results of *Scenario 3* demonstrate that the proposed algorithm in this paper has strong robustness and can be used for complex location scenarios consisting of heterogeneous sensors. The measurements used by different algorithms are distinct. It is not reasonable to compare their performance

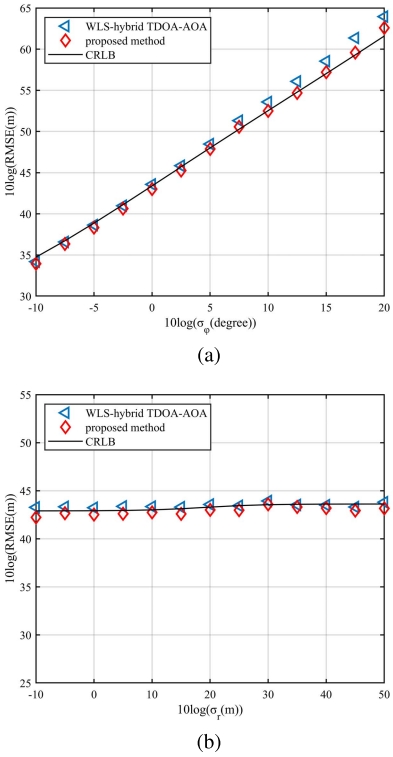

Fig. 9. Localization performance of different algorithms using the same measurements when $\sigma_s = 5\text{m}$, where (a) $\sigma_r = 10\text{m}$; (b) $\sigma_\varphi = 1^\circ$.

directly. Next, we compare the location performance of the two algorithms under the hybrid TDOA and AOA measurement applicable to the WLS hybrid.

Scenario 4: Only the first three stations in *Scenario 3* participate in localization, where each station is configured with the same sensors as the reference station. Comparing the impact of different noises on the performance of the proposed localization method and WLS-hybrid.

Fig. 9 describes the localization performance trend of the two hybrid measurement algorithms with a single noise. Since the number of AOA measurements is three times that of TDOA, the positioning performance of the two algorithms is insensitive to TDOA noise and varies only slightly with TDOA noise. With the increase of AOA noise, WLS-hybrid estimation performance deviates from CRLB, and the performance of the proposed algorithm can always reach CRLB accuracy well. Our algorithm does not introduce the coupling between AOA measurements during the linearization of TDOA measurements with respect to the source position, so it is more resistant to noise.

B. Optimal Geometry

In this subsection, we will verify the conclusion and validity of the optimal geometry.

Scenario 5: We use three stations $\mathbf{s_0} = [r_0, 0]^T$, $\mathbf{s}_1 = [r_1 \cos\lambda_1, r_1 \sin\lambda_1]^T$ and $\mathbf{s}_2 = [r_2 \cos\lambda_2, r_2 \sin\lambda_2]^T$ to locate the source $\mathbf{u} = [0, 0]^T$. $\mathbf{s_0}$ is the reference station. r_o, r_1 and r_2 represent the distance between the source and these stations. Fixing the standard deviation $\sigma_\varphi = 0.1^\circ$ and $\sigma_r = 1\text{m}$ of measurement noise.

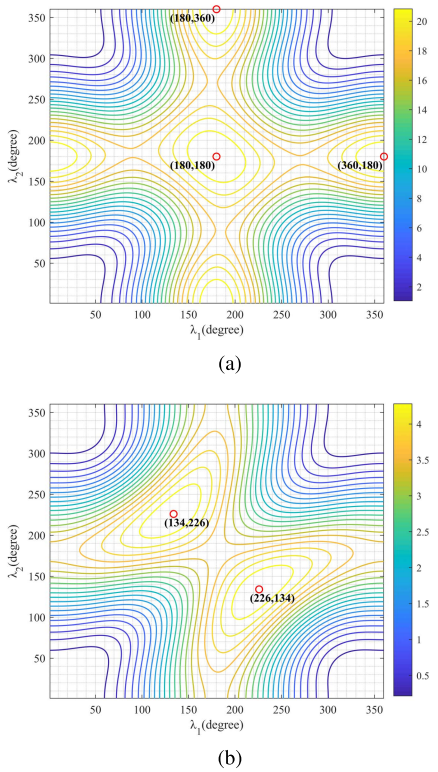

Fig. 10. Contour of $\det(\mathbf{A})$ corresponding to the angular positions λ_1 and λ_2, where (a) $r_0 = 200\text{m}$;(b) $r_0 = 500\text{m}$. Red 'o' indicates the maximum.

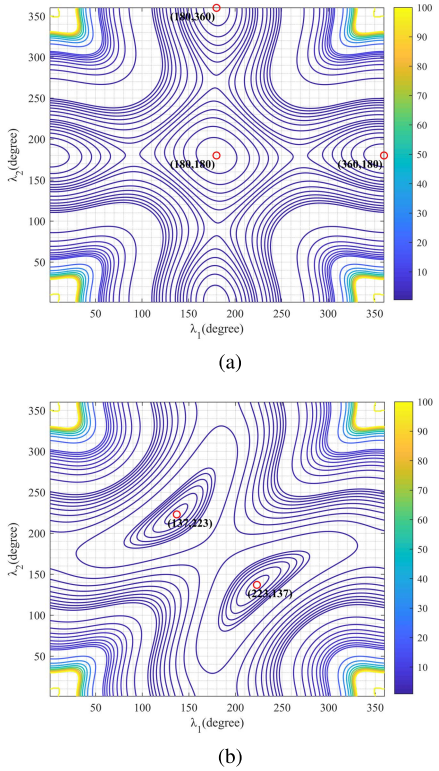

Fig. 11. Contour of $\text{tr}(\text{CRLB})$ corresponding to the angular positions λ_1 and λ_2, where (a) $r_0 = 200\text{m}$;(b) $r_0 = 500\text{m}$. Red 'o' indicates the maximum.

According to *Conclusions 2* and *3*, the critical value of the distance between the reference station and the source is about $r_0 \approx 286\text{m}$. Below, we will verify the conclusion in two cases, $r_0 = 200\text{m}$ and $r_0 = 500\text{m}$. The localization performance depends on the angle positions λ_1 and λ_2 of the two stations, while r_1 and r_2 are not affected.

We evaluate the results of the optimal geometry through an exhaustive numerical search and use the proposed algorithm to prove the effectiveness of the optimal geometry. Substituting the parameter values into *Conclusion 2*, it is easy to obtain that the angular positions of the stations under the optimal geometric configuration are $\lambda_1 = 133.9326°$ and $\lambda_2 = 226.0674°$.

Through two exhaustive methods with step size $1°$, the contour of $\det(\mathbf{A})$ corresponding to the different angular positions are shown in Fig.10. The optimal geometric configurations of $r_0 = 200\text{m}$ and $r_0 = 500\text{m}$ are obtained as $(\lambda_1, \lambda_2) \in \{(180°, 180°), (180°, 0), (0, 180°)\}$ and $(\lambda_1, \lambda_2) \in \{(134°, 226°), (226°, 134°)\}$, respectively, which is the same as *Conclusion 2*.

The geometric configuration of the determinant maximum of the FIM is not exactly equivalent to the trace minimum of CRLB [26]. We calculate the trace of CRLB in two cases by the same exhaustive search method, as shown in Fig.11. The optimal geometry is slightly distinction from D-optimality criterion. The discrepancies between the objective functions lead to subtle differences in the conclusions. The achievable $1/\text{tr}(\text{CRLB})$ is within 99% of the best value of the optimal geometric configuration for λ_1 within 128 to 155 degree and

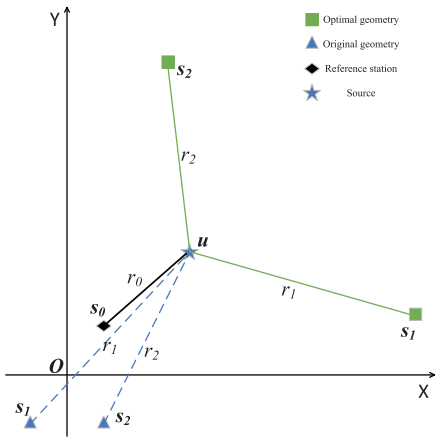

Fig. 12. Schematic diagram of the original and optimal geometric configurations in 2D plane.

λ_2 within 205 to 232 degree [41]. That means our conclusions are valid.

Finally, the optimal geometric configurations it derives cannot be directly proved to be valid for the proposed algorithm.

Based on *Scenario 4*, setting the z-component of each station position as zero to get the 2D localization scenario. Then, fixing the position of the source and reference stations. The distance between the reference station and the source is $r_0 \approx 922\text{m}$. According to *Conclusion 2*, the corresponding optimal layout is $\lambda_0 = 0°$, $\lambda_1 = 124.1804°$ and $\lambda_2 = 235.8196°$. At this point, the angular positions

TABLE III
LOCALIZATION PERFORMANCE OF DIFFERENT GEOMETRIC CONFIGURATIONS IN 2D PLANE

Geometry(2D)	Tr(CRLB)(m^2)	MSE(m^2)	Bias norm(m)
Optimal	2.7488	1.6441	0.0351
Original	62.1327	62.7455	0.3334

of the optimal geometric configuration are equivalent to the azimuth of the source relative to each station in the 2D plane as $\alpha_0 = 40.6013°$, $\alpha_1 = 164.7831°$, and $\alpha_2 = -83.5805°$. The optimal geometric configuration is obtained without changing the stations-source spacings and moving these stations to the corresponding position. The original and optimal geometrical configurations are shown in Fig.12. Table III describes the positioning performance of the two geometric configurations.

Clearly, the results in Table III show that good geometry can greatly improve positioning performance. It is practical to precisely locate the target by changing the geometric configuration without changing the hardware conditions.

VII. CONCLUSION

In the presence of different types of noise, we propose different closed-form solution source localization methods based on hybrid multi-station TDOA and single-station AOA. Theoretical analysis shows that when the noise satisfies conditions C1-C4, these localization methods proposed in this paper can achieve CRLB accuracy. Compared with OLSE, although it has slightly higher computational complexity, it has higher localization accuracy. Compared with IMLE, it has the advantages of low computational complexity and strong stability, and does not require precise initial values. It is demonstrated that our algorithm has stronger robustness than MPR-TDOA, PLE-AOA, and WLS-hybrid by applying them in complex localization scenarios. Using the same measurements, our algorithm is more resistant to noise than WLS-hybrid.

To further improve localization accuracy, we investigate the geometry between the source and the stations. Through theoretical analysis, we give the corresponding explicit solutions for the optimal geometric layout when two or three stations are positioned in concert. The solution for the optimal geometrical configuration when four and more stations are positioned is also given. Simulation experiments demonstrate that the theoretical conclusions are correct and the optimal geometric configuration is effective to improve the positioning performance.

In this paper, we investigate the optimal geometric configuration for 2D positioning scenarios such as the sea surface. It is quite different from 3D. However, the difficulty of solving the optimal geometric configuration increases dramatically from 2D planes to 3D space, because the number of variables doubles and their coupling is very complicated. In the future, our work will focus on the generalized solution of 3D optimal geometric configurations in heterogeneous sensor networks.

APPENDIX A

The definitions of each parameter in the weighted least squares estimation formula (24) are as follows: $\tilde{\mathbf{h}}_{\mathbf{n}} = \left[\tilde{\mathbf{h}}^T, \tilde{\mathbf{h}}_{\mathbf{n}\varphi}^T\right]^T \in \mathbb{R}^{(3N+2)\times 1}$, $\tilde{\mathbf{h}}_{\mathbf{n}\varphi} = \left[\tilde{\mathbf{s}}_0^T\tilde{\gamma}_1, \tilde{\mathbf{s}}_0^T\tilde{\gamma}_2, \cdots, \tilde{\mathbf{s}}_0^T\tilde{\gamma}_N\right]^T \in \mathbb{R}^{2N\times 1}$, $\tilde{\mathbf{G}}_{\mathbf{n}} = \left[\tilde{\mathbf{G}}^T, \tilde{\mathbf{G}}_{\mathbf{n}\varphi}\right]^T \in \mathbb{R}^{(3N+2)\times 3}$, $\tilde{\mathbf{G}}_{\mathbf{n}\varphi} = \left[\tilde{\gamma}_1^T, \tilde{\gamma}_2^T, \cdots, \tilde{\gamma}_N^T\right]^T$, $\tilde{\gamma}_i = \begin{bmatrix} \sin\tilde{\alpha}_i & -\cos\tilde{\alpha}_i & 0 \\ \sin\tilde{\beta}_i\cos\tilde{\alpha}_i & \sin\tilde{\beta}_i\sin\tilde{\alpha}_i & -\cos\tilde{\beta}_i \end{bmatrix}^T$, $\Sigma_{\mathbf{n}} = \left(\mathbf{T}_{\mathbf{n}}\mathbf{Q}_{\mathbf{m_n}}\mathbf{T}_{\mathbf{n}}^T + \mathbf{B}_{\mathbf{n}}\mathbf{Q}_{\mathbf{s}}\mathbf{B}_{\mathbf{n}}^T\right)^{-1}$, $\mathbf{B}_{\mathbf{n}} = \left[\mathbf{B}_{\mathbf{r}}^T, \mathbf{B}_{\varphi_{\mathbf{n}}}^T\right]^T \in \mathbb{R}^{(3N+2)\times(3N+3)}$, $\mathbf{T}_{\mathbf{n}} = \text{blkdiag}\left(\mathbf{T}_{\mathbf{r}}, \mathbf{T}_{\varphi_{\mathbf{n}}}\right) \in \mathbb{R}^{(3N+2)\times(3N+2)}$, $\mathbf{Q}_{\mathbf{m_n}} = \text{blkdiag}(\mathbf{Q}_{\mathbf{r}}, \mathbf{Q}_{\varphi_{\mathbf{n}}})$, $\mathbf{B}_{\varphi_{\mathbf{n}}} = \text{blkdiag}\left(\gamma_0^T, \gamma_1^T, \cdots, \gamma_N^T\right) \in \mathbb{R}^{(2N+2)\times(3N+3)}$, $\mathbf{T}_{\varphi_{\mathbf{n}}} = \text{diag}\left([r_0\cos\beta, r_0, \cdots, r_N\cos\beta, r_N]\right)$, $\mathbf{Q}_{\varphi_{\mathbf{n}}} = \text{diag}\left(\left[\sigma_{\alpha_0}^2, \sigma_{\beta_0}^2, \cdots, \sigma_{\alpha_N}^2, \sigma_{\beta_N}^2\right]\right)$.

APPENDIX B

In this Appendix, we will demonstrate that the localization performance of the proposed method can reach CRLB accuracy under small noise conditions.

According to the definitions of matrices $\mathbf{G_m}$ in (11), $\mathbf{T}$ in (12) and $\nabla_{\mathbf{mu}}$ in (26), it is easy to get

$$\mathbf{T^{-1}G_m} = \begin{bmatrix} \mathbf{T_r^{-1}} & \mathbf{0} \\ \mathbf{0} & \mathbf{T}_\varphi^{-1} \end{bmatrix} \begin{bmatrix} \mathbf{G_{mr}} \\ \mathbf{G_{m\varphi}} \end{bmatrix} = \begin{bmatrix} \mathbf{T_r^{-1}G_{mr}} \\ \mathbf{T}_\varphi^{-1}\mathbf{G_{m\varphi}} \end{bmatrix} = \nabla_{\mathbf{mu}}. \tag{43}$$

From (31) and (26), it is easy to obtain

$$\text{cov}_{\mathbf{m}}(\mathbf{u}) = \text{CRLB}_{\mathbf{m}}(\mathbf{u}). \tag{44}$$

When both measurement error and station position error exist, the covariance matrix of source position estimation is inversely calculated to obtain

$$\begin{aligned} &\text{cov}_{\mathbf{b}}(\mathbf{u})^{-1} \\ &= \mathbf{G}^T\left(\mathbf{T}\mathbf{Q_m}\mathbf{T}^T + \mathbf{B}\mathbf{Q_s}\mathbf{B}^T\right)^{-1}\mathbf{G} \\ &= \mathbf{G}^T\mathbf{T}^{-T}\left(\mathbf{Q_m} + \mathbf{T}^{-1}\mathbf{B}\mathbf{Q_s}\mathbf{B}^T\mathbf{T}^{-T}\right)^{-1}\mathbf{T}^{-1}\mathbf{G} \\ &= \mathbf{G}^T\mathbf{T}^{-T}\mathbf{Q_m^{-1}}\mathbf{T}^{-1}\mathbf{G} - \mathbf{G}^T\mathbf{T}^{-T}\mathbf{Q_m^{-1}}\mathbf{T}^{-1}\mathbf{B} \\ &\quad \times\left(\mathbf{Q_s^{-1}} + \mathbf{B}^T\mathbf{T}^{-T}\mathbf{Q_m^{-1}}\mathbf{T}^{-1}\mathbf{B}\right)^{-1} \times \mathbf{B}^T\mathbf{T}^{-T}\mathbf{Q_m^{-1}}\mathbf{T}^{-1}\mathbf{G}. \end{aligned} \tag{45}$$

According to the definitions of matrices $\mathbf{T}$ in (12), $\mathbf{B}$ in (18) and $\nabla_{\mathbf{ms}}$ in (27), it is easy to get

$$\mathbf{T^{-1}B} = \begin{bmatrix} \mathbf{T_r^{-1}} & \mathbf{0} \\ \mathbf{0} & \mathbf{T}_\varphi^{-1} \end{bmatrix} \begin{bmatrix} \mathbf{B_r} \\ \mathbf{B}_\varphi \end{bmatrix} = \begin{bmatrix} \mathbf{T_r^{-1}B_r} \\ \mathbf{T}_\varphi^{-1}\mathbf{B}_\varphi \end{bmatrix} = -\nabla_{\mathbf{ms}}. \tag{46}$$

Since $\mathbf{G} = \mathbf{G_m}$, it follows that $\mathbf{T^{-1}G} = \nabla_{\mathbf{mu}}$.

Similarly, from (28) and (33), it is easy to obtain

$$\text{cov}_{\mathbf{b}}(\mathbf{u}) = \text{CRLB}_{\mathbf{b}}(\mathbf{u}). \tag{47}$$

The proposed solution achieves CRLB accuracy in the small error region satisfying conditions (C1)-(C4).

APPENDIX C
OPTIMAL GEOMETRY FOR $N = 1$ AND $N = 2$

When $N = 1$, the optimal geometric configurations of the two parts of (42) are consistent. The maximum value of $\det(\mathbf{A})$ is $\frac{2}{r_0^2\sigma_\varphi^2\sigma_r^2}$, when the angular position of the two stations satisfy $\lambda_1 = \pi + \lambda_0$.

In addition, r_0 should be as small as possible since $\det(\mathbf{A})$ is negatively correlated to the distance from the source to the reference station. The same is true below.

When $N = 2$, the optimal geometric configurations of the two parts of (42) are inconsistent. According to the constraints in (41), the angular positions of stations 1 and 2 satisfy $\lambda_1 + \lambda_2 = 2\pi$ and $\sin\lambda_i = 0, i = 1, 2$.

If the angular positions are $\sin\lambda_i = 0, i = 1, 2$, from(42), the objective function becomes

$$\max_{\lambda_i, i=1,2,\ldots,N} \frac{1}{3r_0^2\sigma_\varphi^2\sigma_r^2}\left[3\sum_{i=0}^{2}\cos^2\lambda_i - \left(\sum_{i=0}^{2}\cos\lambda_i\right)^2\right] \quad \mathbf{s.t.} \quad \sin\lambda_i = 0, i = 0, 1, 2. \tag{48}$$

It is easy to get the angular positions of optimal geometric $\lambda_1 = \pi + \lambda_0, \lambda_2 = \lambda_0$ (λ_1 and λ_2 are interchangeable when the noise distribution is the same).

If $\lambda_1 + \lambda_2 = 2\pi$, we let $\cos\lambda_1 = \cos\lambda_2 = a$, $a \in [-1, 1]$. From (42), the objective function becomes

$$\max_a \frac{4(1-a)^3(1+a)}{3\sigma_r^4} + \frac{2(1-a)^2}{3r_0^2\sigma_\varphi^2\sigma_r^2}. \tag{49}$$

Analyzing its derivative, we get the following conclusions: When $r_o \le \sigma_r/2\sigma_\varphi$, $a = -1$ maximizes (49), and the optimal geometry is $\lambda_1 = \lambda_2 = \pi + \lambda_0$. When $r_0 > \sigma_r/2\sigma_\varphi$, $a = 1/4 - \sqrt{9/16 + \sigma_r^2/\left(4r_0^2\sigma_\varphi^2\right)}$ maximizes (49), and the angular positions of the stations are $\lambda_1 = \cos^{-1}a + \lambda_0, \lambda_2 = 2\pi - \cos^{-1}a + \lambda_0$.

REFERENCES

[1] T.-K. Le and N. Ono, "Closed-form and near closed-form solutions for TDOA-based joint source and sensor localization," *IEEE Trans. Signal Process.*, vol. 65, no. 5, pp. 1207–1221, Mar. 2017.

[2] H. Shen, Z. Ding, S. Dasgupta, and C. Zhao, "Multiple source localization in wireless sensor networks based on time of arrival measurement," *IEEE Trans. Signal Process.*, vol. 62, no. 8, pp. 1938–1949, Apr. 2014.

[3] Y. T. Chan and K. C. Ho, "A simple and efficient estimator for hyperbolic location," *IEEE Trans. Signal Process.*, vol. 42, no. 8, pp. 1905–1915, Aug. 1994.

[4] K. W. K. Lui, F. K. W. Chan, and H. C. So, "Semidefinite programming approach for range-difference based source localization," *IEEE Trans. Signal Process.*, vol. 57, no. 4, pp. 1630–1633, Apr. 2009.

[5] K. Yang, G. Wang, and Z.-Q. Luo, "Efficient convex relaxation methods for robust target localization by a sensor network using time differences of arrivals," *IEEE Trans. Signal Process.*, vol. 57, no. 7, pp. 2775–2784, Jul. 2009.

[6] J.-A. Luo, X.-P. Zhang, and Z. Wang, "A new passive source localization method using AOA-GROA-TDOA in wireless sensor array networks and its Cramér-Rao bound analysis," in *Proc. IEEE Int. Conf. Acoust., Speech Signal Process.*, 2013, pp. 4031–4035.

[7] K. Doğançay, "3D pseudolinear target motion analysis from angle measurements," *IEEE Trans. Signal Process.*, vol. 63, no. 6, pp. 1570–1580, Mar. 2015.

[8] Y. Wang and K. C. Ho, "Unified near-field and far-field localization for AOA and hybrid AOA-TDOA positionings," *IEEE Trans. Wireless Commun.*, vol. 17, no. 2, pp. 1242–1254, Feb. 2018.

[9] Y.-Y. Li, G.-Q. Qi, and A.-D. Sheng, "Performance metric on the best achievable accuracy for hybrid TOA/AOA target localization," *IEEE Commun. Lett.*, vol. 22, no. 7, pp. 1474–1477, Jul. 2018.

[10] L. Badriasl, H. Kennedy, and A. Finn, "Effects of coordinate system rotation on two novel closed-from localization estimators using azimuth/elevation," in *Proc. 16th Int. Conf. Inf. Fusion*, 2013, pp. 1797–1804.

[11] A. N. Bishop, B. Fidan, and K. Doanay, "Exploiting geometry for improved hybrid AOA/TDOA-based localization," *Signal Process.*, vol. 88, no. 7, pp. 1775–1791, 2008.

[12] R. Amiri, F. Behnia, and H. Zamani, "Efficient 3-D positioning using time-delay and AOA measurements in MIMO radar systems," *IEEE Commun. Lett.*, vol. 21, no. 12, pp. 2614–2617, Dec. 2017.

[13] K. C. Ho, "Bias reduction for an explicit solution of source localization using TDOA," *IEEE Trans. Signal Process.*, vol. 60, no. 5, pp. 2101–2114, May 2012.

[14] G. Wang and K. C. Ho, "Convex relaxation methods for unified near-field and far-field TDOA-based localization," *IEEE Trans. Wireless Commun.*, vol. 18, no. 4, pp. 2346–2360, Mar. 2019.

[15] M. Malanowski and K. Kulpa, "Two methods for target localization in multistatic passive radar," *IEEE Trans. Aerosp. Electron. Syst.*, vol. 48, no. 1, pp. 572–580, Jan. 2012.

[16] G. Bai, J. Liu, Y. Song, and Y. Zuo, "Two-UAV intersection localization system based on the airborne optoelectronic platform," *Sensors*, vol. 17, no. 1, p. 98, Jan. 2017.

[17] Y. Wang and K. C. Ho, "An asymptotically efficient estimator in closed-form for 3-D AOA localization using a sensor network," *IEEE Trans. Wireless Commun.*, vol. 14, no. 12, pp. 6524–6535, Dec. 2015.

[18] L. Cong and W. Zhuang, "Hybrid TDOA/AOA mobile user location for wideband CDMA cellular systems," *IEEE Trans. Wireless Commun.*, vol. 1, no. 3, pp. 439–447, Jul. 2002.

[19] J. Yin, Q. Wan, S. Yang, and K. C. Ho, "A simple and accurate TDOA-AOA localization method using two stations," *IEEE Signal Process. Lett.*, vol. 23, no. 1, pp. 144–148, Jan. 2016.

[20] F. Zhang, Y. Sun, and Q. Wan, "Calibrating the error from sensor position uncertainty in TDOA-AOA localization," *Signal Process.*, vol. 166, Jan. 2020, Art. no. 107213.

[21] T. Jia, H. Wang, X. Shen, Z. Jiang, and K. He, "Target localization based on structured total least squares with hybrid TDOA-AOA measurements," *Signal Process.*, vol. 143, pp. 211–221, Feb. 2018.

[22] A. N. Bishop, B. Fidan, B. D. O. Anderson, K. Doğançay, and P. N. Pathirana, "Optimality analysis of sensor-target localization geometries," *Automatica*, vol. 46, no. 3, pp. 479–492, Mar. 2010.

[23] S. Zhao, B. M. Chen, and T. H. Lee, "Optimal sensor placement for target localisation and tracking in 2D and 3D," *Int. J. Control*, vol. 86, no. 10, pp. 1687–1704, 2013.

[24] W. Meng, L. Xie, and W. Xiao, "Optimal TDOA sensor-pair placement with uncertainty in source location," *IEEE Trans. Veh. Technol.*, vol. 65, no. 11, pp. 9260–9271, Nov. 2016.

[25] S. Xu and K. Doğançay, "Optimal sensor placement for 3-D angle-of-arrival target localization," *IEEE Trans. Aerosp. Electron. Syst.*, vol. 53, no. 3, pp. 1196–1211, Jun. 2017.

[26] D. Moreno-Salinas, A. Pascoal, and J. Aranda, "Optimal sensor placement for acoustic underwater target positioning with range-only measurements," *IEEE J. Ocean. Eng.*, vol. 41, no. 3, pp. 620–643, Jul. 2016.

[27] N. H. Nguyen and K. Doğançay, "Optimal geometry analysis for multistatic TOA localization," *IEEE Trans. Signal Process.*, vol. 64, no. 16, pp. 4180–4193, Aug. 2016.

[28] Y.-H. Kim, D.-G. Kim, K.-H. Song, H.-N. Kim, and J. W. Han, "Analysis of sensor-emitter geometry for emitter localisation using TDOA and FDOA measurements," *IET Radar, Sonar Navigat.*, vol. 11, pp. 341–349, Feb. 2017.

[29] W. Meng, L. Xie, and W. Xiao, "Optimality analysis of sensor-source geometries in heterogeneous sensor networks," *IEEE Trans. Wireless Commun.*, vol. 12, no. 4, pp. 1958–1967, Apr. 2013.

[30] M. Sadeghi, F. Behnia, and R. Amiri, "Optimal geometry analysis for TDOA-based localization under communication constraints," *IEEE Trans. Aerosp. Electron. Syst.*, vol. 57, no. 5, pp. 3096–3106, Oct. 2021.

[31] E. Tzoreff and A. J. Weiss, "Path design for best emitter location using two mobile sensors," *IEEE Trans. Signal Process.*, vol. 65, no. 19, pp. 5249–5261, Oct. 2017.

[32] Y. Wang and K. C. Ho, "TDOA positioning irrespective of source range," *IEEE Trans. Signal Process.*, vol. 65, no. 6, pp. 1447–1460, Mar. 2017.

[33] P. Stoica and K. C. Sharman, "Maximum likelihood methods for direction-of-arrival estimation," *IEEE Trans. Acoust., Speech, Signal Process.*, vol. 38, no. 7, pp. 1132–1143, Jul. 1990.

[34] X. Qu and L. Xie, "Source localization by TDOA with random sensor position errors—Part II: Mobile sensors," in *Proc. 15th Int. Conf. Inf. Fusion*, 2012, pp. 54–59.
[35] K. Dogancay, "Bias compensation for the bearings-only pseudolinear target track estimator," *IEEE Trans. Signal Process.*, vol. 54, no. 1, pp. 59–68, Jan. 2006.
[36] S. M. Kay, *Fundamentals of Statistical Signal Processing: Estimation Theory*. Upper Saddle River, NJ, USA: Prentice-Hall, 1993.
[37] S. Arora and B. Barak, *Computational Complexity: A Modern Approach*. Cambridge, U.K.: Cambridge Univ. Press, 2009.
[38] C. Yang, L. Kaplan, and E. Blasch, "Performance measures of covariance and information matrices in resource management for target state estimation," *IEEE Trans. Aerosp. Electron. Syst.*, vol. 48, no. 3, pp. 2594–2613, Jul. 2012.
[39] D. Ucinski, *Optimal Measurement Methods for Distributed Parameter System Identification*. Boca Raton, FL, USA: CRC Press, 2004.
[40] Y. Sun, K. C. Ho, and Q. Wan, "Solution and analysis of TDOA localization of a near or distant source in closed form," *IEEE Trans. Signal Process.*, vol. 67, no. 2, pp. 320–335, Jan. 2019.
[41] Y. Zhang and K. C. Ho, "Multistatic localization in the absence of transmitter position," *IEEE Trans. Signal Process.*, vol. 67, no. 18, pp. 4745–4760, Sep. 2019.

Xu Kang received the B.S. degree in physics from Zhengzhou University, Zhengzhou, China, in 2019. He is currently pursuing the Ph.D. degree in optical engineering with the Changchun Institute of Optics, Fine Mechanics and Physics, Chinese Academy of Sciences, Changchun, China. His main research interests include target localization, sensor placement optimization, and statistical signal processing.

Dejiang Wang received the B.S. degree in communication engineering from Nankai University, Tianjin, China, in 2004, the M.S. degree in electronic engineering from Tsinghua University, Beijing, China, in 2007, and the Ph.D. degree in optical engineering from the Changchun Institute of Optics, Fine Mechanics and Physics, Chinese Academy of Sciences, Changchun, China, in 2013.

He is currently a Research Fellow with the Changchun Institute of Optics, Fine Mechanics and Physics, Chinese Academy of Sciences. His research interests include signal processing, infrared image processing, and pattern recognition.

Yu Shao received the B.S. degree in optoelectronic information science and technology and engineering from Shanxi University, Taiyuan, China, in 2019. He is currently pursuing the Ph.D. degree in optical engineering with the Changchun Institute of Optics, Fine Mechanics and Physics, Chinese Academy of Sciences, Changchun, China. His current research interests include digital image processing.

Mingyang Ma received the B.S. degree from the Changchun University of Science and Technology, Changchun, China, in 2017, and the Ph.D. degree from the Changchun Institute of Optics, Fine Mechanics and Physics, Chinese Academy of Sciences, Changchun, in 2022.

He is currently a Post-Doctoral Researcher with the Key Laboratory of Airborne Optical Imaging and Measurement, Chinese Academy of Sciences. His main research interests include statistical signal processing, estimation theory, and sensor data fusion.

Tao Zhang received the B.E. degree from Zhejiang University in 1987.

From 1987 to 2008, he was the Deputy Researcher of the Photoelectric Engineering Department, the Deputy Director of the Scientific Research Department, the Director of the Optical Engineering Center, the Deputy Director of the Photoelectric Engineering Department, a Researcher and the Director of the Aviation Surveillance Department, and the General Manager of the Opp Photoelectric Technology Company Ltd., Changchun Institute of Optics, Fine Mechanics and Physics, Chinese Academy of Sciences. From 2008 to 2012, he was the Deputy Group Leader of the Preparation Team, Suzhou Institute of Biomedical Engineering Technology (preparatory), Chinese Academy of Sciences, and the Director of the Medical Image Technology Research Department (concurrently: an Assistant Director with the Changchun Institute of Optics, Fine Mechanics and Physics, Chinese Academy of Sciences, in 2010). He has been the Vice President of the Changchun Optical Machinery Institute since 2012. His research interests include detection and imaging technology and stability control technology.

Dr. Zhang received the two Second-Class Prizes for scientific and technological progress from the Chinese Academy of Sciences, the one Third-Class Prize for scientific and technological progress from the Chinese Academy of Sciences, as well as the one National Invention Patent Award, and enjoys the government subsidy of the State Council.